J Mater Sci (2010) 45:2258–2263
DOI 10.1007/s10853-009-4126-z

On the microstructure of single wall carbon nanotubes reinforced ceramic matrix composites

E. Zapata-Solvas · D. Gómez-García · A. Domínguez-Rodríguez

Received: 29 September 2009 / Accepted: 10 December 2009 / Published online: 9 February 2010

Abstract A microstructural modelling of the microstructure in single wall carbon nanotubes reinforced alumina ceramics has been developed. The model accounts for the main microstructural features, being quite useful to describe the carbon nanotube distribution along the ceramic matrix. The microstructural analysis derived from this model is found to give a deeper insight into the high-temperature creep of these composites.

Introduction

Since Iijima discovered carbon nanotubes (CNTs) [1], there has been a growing interest in the study of the structure and properties of CNTs [2–5]. Particularly over the past decade an intense effort has been carried out in ceramic matrix composites with single wall carbon nanotubes (SWCNTs). This interest stems from the idea that one can impart some of attractive properties of the SWCNTs to the ceramic matrix composites, resulting in materials with interesting properties, such as mechanical [6, 7], electrical [8, 9], thermal [10] and thermoelectric [11] properties. One of the most studied properties are the mechanical ones, due to the exceptional SWCNTs stiffness and strength [2, 12–15]. Physical properties of polycrystalline ceramics depend on grain boundaries structure [16]. In ceramic matrix composites with SWCNTs, grain boundaries can be engineered by the adequate control of the SWCNTs dispersion into the ceramic matrix. Different dispersion routines have been performed to increase the dispersion grade of SWCNTs and to avoid bundles of nanotubes driven by Van der Waals attraction [17–24]. SWCNTs are distributed along ceramic matrix grain boundaries, Padture et al. [25] explain the SWCNTs distribution as 3D network of a 2D mat comprising entangled 1D SWCNTs bundles. Recently, in a small angle neutron scattering, Koszor et al. [26] showed that predominant part of SWCNTs can be found in loose networks surrounding the ceramic matrix grains. In this work, a modelling of SWCNTs distribution along grain boundaries will be discussed. A relationship between SWCNTs volume fraction f, ceramic matrix grain size d, mean SWCNTs bundles diameter w and ceramic matrix grain surface fraction without contact with SWCNTs (Φ) will be developed. Quantitative microstructural data measured by transmission electron microscopy (TEM) and electron energy loss spectroscopy (EELS) will be carried out to prove the developed model validity and its application to understand high temperature mechanical properties of Al_2O_3/SWCNTs composites.

Experimental procedure and results

Sample preparation

Two sets of composites were fabricated: Al_2O_3/SWNTs and Al_2O_3/acid-treated SWNTs (TSWNTs); the difference being in the dispersion routine. The fabrication of the Al_2O_3/SWNTs composite is described in a previous study [6], and the as-received SWNTs were dispersed in a methanol solution with Al_2O_3 nanopowders; with the aid of ultrasonic agitation, yielding in 90 vol% Al_2O_3 + 10 vol% SWNTs in the solution, followed by Spark Plasma Sintering (SPS) at 1350 °C and 5-min holding time. In the

E. Zapata-Solvas (✉) · D. Gómez-García · A. Domínguez-Rodríguez
Departamento de Física de la Materia Condensada, Universidad de Sevilla, ICMSE-CSIC, Apartado 1065, 41080 Sevilla, Spain
e-mail: ezapata@us.es

acid-treated sample an aqueous colloidal processing with a SWNTs acid-treatment are carried out as dispersion routine [19], the SWNTs volume fraction and SPS sintering are identically than Al_2O_3/SWNTs sample. Densities were measured using Archimedes method resulting in 94.9 and 97.6% for Al_2O_3/SWNTs and Al_2O_3/TSWNTs, respectively. The theoretical density values for the composites were obtained from the literature, which are based-on-rule of mixtures calculation using the following density values [27]: Al_2O_3 3.97 g/cm^3 and SWNTs 1.80 g/cm^3.

Microstructural characterisation

Grain size measurements were carried out in a previous work by TEM [28]: grain size values of 0.83 ± 0.07 and 0.50 ± 0.04 μm were measured for Al_2O_3/SWCNTs and Al_2O_3/TSWCNTs composites, respectively. Grain size was defined by $d = 1.56L$, where L is the mean interception length. This grain size definition is usually used in alumina ceramics [29]. Carbon maps were obtained by EELS for both composites to measure the width of SWCNTs phase w and alumina grain surface fraction (A) under contact with SWCNTs. The width of SWCNTs phase w range, obtained by EELS and TEM, is 2 nm $< w <$ 0.2 μm and 24 nm $< w <$ 1.5 μm for Al_2O_3/SWCNTs and Al_2O_3/TSWCNTs composites [30], respectively. The mean SWCNTs width phase w measured for Al_2O_3/TSWCNTs composite is 24 ± 8 nm and $w = 120 \pm 40$ nm for Al_2O_3/SWCNTs composites using EELS carbon maps [28]. The EELS carbon maps were acquired in a CM200 (Philips Electron Optics, Eindhoven, The Netherlands) operated at 200 kV and at EELS lowest magnification, which was not enough to characterise regions with agglomerated SWNTs presence. This magnification is suitable to characterise width of SWNTs bundles up to 300 nm in order to acquire a map with more than 15 grains and its boundaries, with the aim of obtain a precise statistical assessment. A correction using Bright Field imaging in the latter TEM microscope was performed, obtaining after that a value of $w = 300 \pm 100$ nm. Agglomerated SWNTs in Al_2O_3/SWNTs composite can be observed in Fig. 1. For further details about EELS see Ref. [28]. Values of $P = 0.27 \pm 0.03$ and $P = 0.81 \pm 0.08$ were measured for alumina grain perimeter fraction under contact with SWCNTs P for Al_2O_3/SWCNTs and Al_2O_3/TSWCNTs composites [30], respectively.

Modelling and discussion

Assuming a homogeneous SWCNTs distribution, a 2D picture of the system based on a projected area modelling is shown in Fig. 2. Prismatic hexagonal grains, with mean grain size d and the height of layer thickness, L, are considered. Cylindrical SWCNTs, with mean diameter w are also modelled, as depicted in Fig. 2. With these assumptions, the volume fraction of SWCNTs f can be written as follows:

$$f = \frac{n\pi w^2 L}{n\pi w^2 L + \frac{\sqrt{3}}{2} d^2 L} = \frac{n\pi w^2}{n\pi w^2 + \frac{\sqrt{3}}{2} d^2} \quad (1)$$

where n is the mean number of nanotubes per hexagonal grain.

The surface fraction of Al_2O_3 grain boundaries under contact with SWCNTs can be written as follows since a projected SWNTs area on Al_2O_3 grain surfaces, as an assumption of the contact geometry, was made:

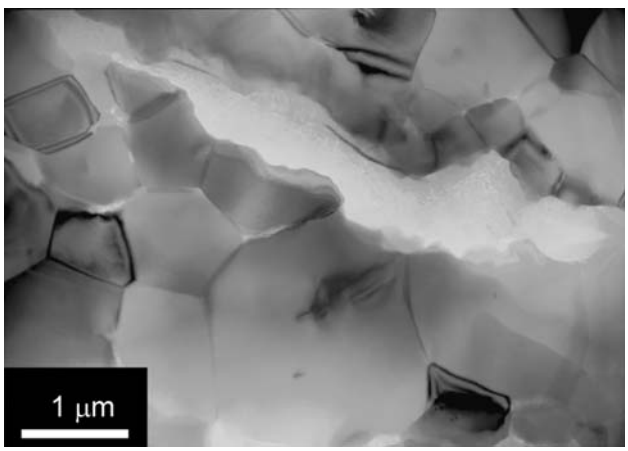

Fig. 1 Bright Field TEM picture showing SWNTs agglomeration in Al_2O_3/SWNTs composites

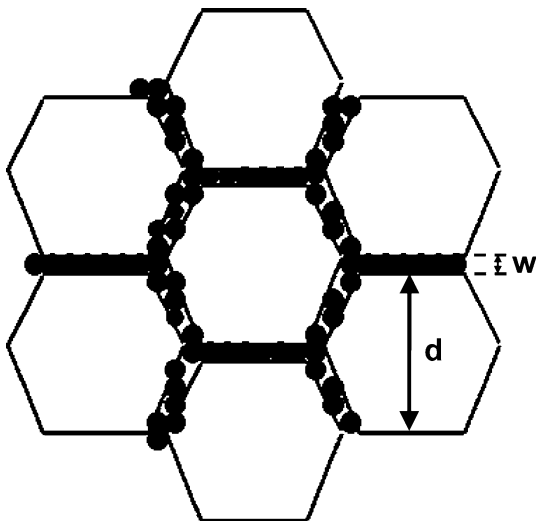

Fig. 2 Schematic picture of a 2D model layer of Al_2O_3 grains and SWNTs modelling

$$A = \frac{\pi n w L}{6\frac{d}{\sqrt{3}}L} = \frac{\pi n w}{2\sqrt{3}d} \tag{2}$$

Thus, a closed expression between A and f can be achieved:

$$A = \frac{f}{\frac{4w}{d}(1-f)} \tag{3}$$

The surface fraction of Al_2O_3 grains without contact with SWCNTs $\Phi = 1 - A$, written as follows:

$$\Phi = \frac{\frac{4w}{d} - f\left(1 + \frac{4w}{d}\right)}{\frac{4w}{d}(1-f)} \tag{4}$$

Obviously, when $\Phi = 0$ no Al_2O_3 free surface is found. This fact is SWCNTs diameter dependent. In a real SWCNTs distribution, the SWCNTs diameter has to be changed for the mean SWCNTs width phase, due to agglomeration by Van der Waals forces [18, 19] of SWCNTs during composites fabrication. In order to study the quality dispersion of SWCNTs, a relationship between the f and Φ follows from (4):

$$f = \frac{\frac{4w}{d}(1-\Phi)}{1 + \frac{4w}{d}(1-\Phi)} \tag{5}$$

Equation 5 can be understood as a relationship between the volume fraction and SWCNTs width phase for a specific value of surface fraction Φ and grain size d. Other geometrical configurations were developed. A thorough analysis shows that the factor 4 obtained in hexagonal geometry ranges between $2\sqrt{2}$ and $4\sqrt{3}$ for different geometries. Hexagonal geometry was chosen because it provides a useful and simple view of the problem. With this geometrical assumption, the surface fraction of Al_2O_3 grain boundaries under contact with SWCNTs is calculated from Al_2O_3 grain perimeter fraction under contact with SWCNTs (P). The perimeter fraction squared is the surface fraction. Alumina grain surface fraction without contact with SWCNTs Φ can be calculated as $1 - A$. Therefore, values of $\Phi = 0.93 \pm 0.02$ and $\Phi = 0.34 \pm 0.08$ were obtained for Al_2O_3/SWCNTs and Al_2O_3/TSWCNTs composites, respectively. A plot of volume fraction versus the mean SWCNTs width is shown in Fig. 3a for different values of surface fraction Φ and grain size d. In this model, for 0.8% of volume fraction all the Al_2O_3 grain boundaries are completely covered by SWCNTs admitted 1 nm SWCNTs diameter. This is not the case in a real system because of the presence of agglomerated SWCNTs. These agglomerated SWCNTs can be imagined as a SWNT with a diameter equal to the bundle width. In Table 1 the SWCNTs bundle width w, surface fraction Φ and grain size d measured by TEM and EELS in Al_2O_3/SWNTs and Al_2O_3/TSWNTs composites are shown. The values of volume fraction f, grain size d and surface fraction Φ of

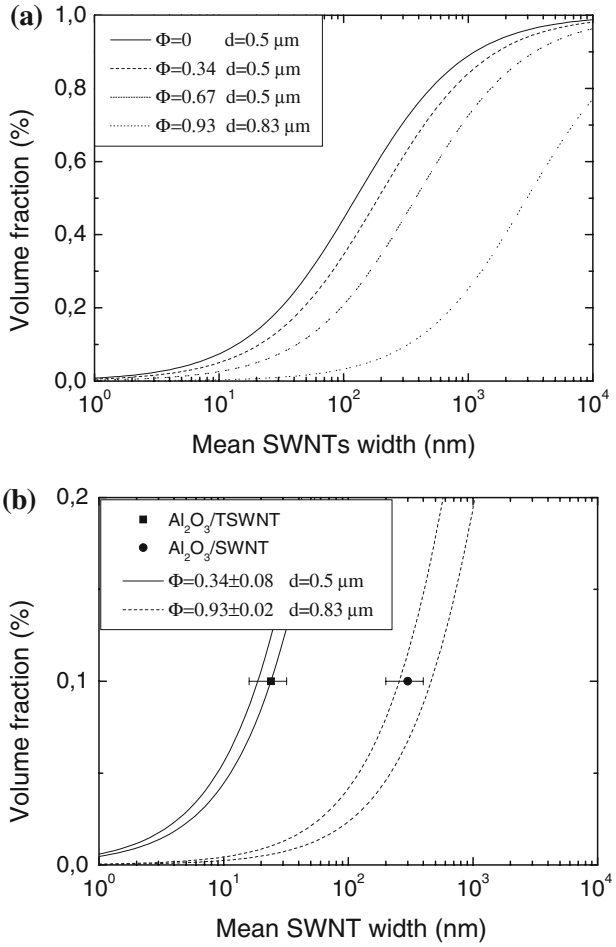

Fig. 3 **a** Theoretical model plot; volume fraction versus mean SWCNTs width for different values of surface fraction Φ and grain sizes d. **b** Correlation between experimental values of mean SWCNTs width and theoretical model developed for Al_2O_3/SWNTs and Al_2O_3/TSWNTs composites

Table 1 SWCNTs bundle width w, surface fraction Φ and grain size d for Al_2O_3/SWCNTs and Al_2O_3/TSWCNTs composites

Composite	SWCNTs width w (nm)	Surface fraction Φ	Grain size d (μm)
Al_2O_3/SWCNTs	300 ± 100	0.93 ± 0.02	0.83 ± 0.07
Al_2O_3/TSWCNTs	24 ± 8	0.34 ± 0.08	0.50 ± 0.04

Al_2O_3/SWNTs and Al_2O_3/TSWNTs composites can be used to prove the validity of the developed model. A plot of theoretical and experimental values of Al_2O_3/SWNTs and Al_2O_3/TSWNTs composites volume fraction versus SWCNTs width phase w is shown in Fig. 3b, including the tolerance of surface fraction Φ carried out in the theoretical calculations and the tolerance of SWCNTs width phase w. A good agreement between theoretical calculations and experimental values prove the model validity.

Application to high temperature creep

All existing high temperature creep results are interpreted in terms of the conventional creep equation [31]:

$$\dot{\varepsilon} = A\frac{Gb}{kT}\left(\frac{b}{d}\right)^{p}\left(\frac{\sigma}{G}\right)^{n} D_0 \exp\left(-\frac{Q}{kT}\right) \quad (6)$$

where $\dot{\varepsilon}$ is the strain rate, A dimensionless constant, G the shear modulus, b the magnitude of the Burgers vectors, k the Boltzmann′s constant, T the absolute temperature, σ the applied stress and d is the average grain size. The term D_0 is the frequency factor of an appropriate diffusion coefficient, whose Arrhenius dependence includes the corresponding activation energy Q. This diffusion coefficient is the one for the migrating species involved in the accommodation process. The parameters p and n, respectively, the grain size and the stress exponent, as well as the activation energy Q, and the microstructural changes after deformation are the fingerprints of possible deformation mechanisms. In our work all the creep data have been fitted to Eq. 6.

In a previous work, high temperature creep tests under uniaxial compression stress were performed. The temperatures used were selected to be high enough for diffusion processes to occur, but sufficiently low to avoid grain growth. Argon gas atmosphere was used in order to avoid oxidation of the SWNTs [7, 28]. The composites were characterised using Raman spectroscopy with the aim of detecting SWNTs presence after creep tests [7]. All this data can be summarised as follows. An stress exponent close to 3 and an activation energy of about 680 kJ/mol were obtained for Al_2O_3/SWCNTs and Al_2O_3/TSWCNTs composites and at the same stress and temperature the Al_2O_3/TSWCNTs composite shows a 3 times higher creep resistance than Al_2O_3/SWCNTs composite as is shown in Fig. 4. Microstructure of Al_2O_3/SWNTs and Al_2O_3/TSWNTs composites before and after deformation can be observed in Fig. 5. Dislocation density was measured and dislocation slide were identified as deformation mechanism in Al_2O_3/SWCNTs and Al_2O_3/TSWCNTs composites [7, 28]. One can understand these results in terms of SWCNTs agglomeration in both composites, or alumina grain surface fraction without contact with SWCNTs Φ. The dislocation density ρ would fit to the critical resolved shear stress τ through Friedel′s law [32] as follows:

$$\tau = CGb\sqrt{\rho} \quad (7)$$

where b is the dislocations Burgers vector and C is a material constant, between 0.2 and 0.5 [33]. The critical resolved stress τ is the applied stress σ multiplied by Schmidt factor, a mean value for the Schmidt factor of a polycrystal can be around 1/3, so Eq. 7 becomes:

$$\sigma \cong Gb\sqrt{\rho} \quad (8)$$

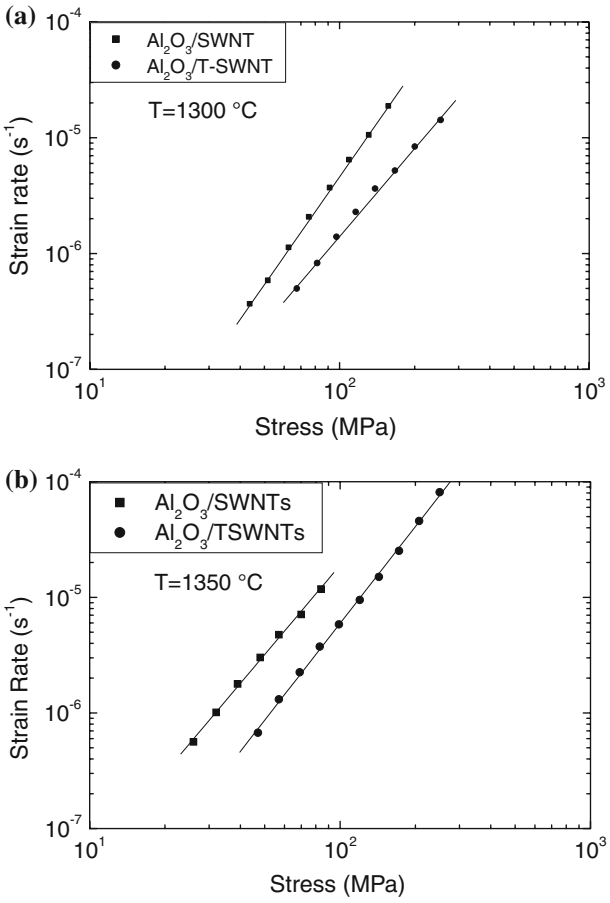

Fig. 4 Plots of high temperature steady-state creep rate ($\dot{\varepsilon}$) versus applied stress (σ) data for the Al_2O_3/SWCNTs and Al_2O_3/TSWCNTs composites at: **a** 1300 °C and **b** 1350 °C

SWCNTs phase acts as rigid phase. In consequence, the Al_2O_3 phase has a restricted mobility, since a high fraction of grains are under contact with one or more SWCNTs phase regions. This fact is a strong restriction for grain boundary mobility, inhibiting grain boundary sliding. Thus, the main mechanism for plasticity is intragranular deformation of alumina grains through recovery creep. The applied stress has a relationship with dislocation density given by Eq. 8. Therefore, the recovery dislocation velocity V [34] will be proportional to the effective diffusion coefficient, applied stress and number of free sinks (points which can act as source of defects for dislocation glide or dislocation annihilation, which are proportional to surface fraction of Al_2O_3 grains surface without contact with SWNTs Φ) as follows,

$$V \propto \frac{D_{\text{eff}}}{kT}\Phi\sigma \quad (9)$$

where k is the Boltzmann constant. The Orowan′s law [31] can be written as,

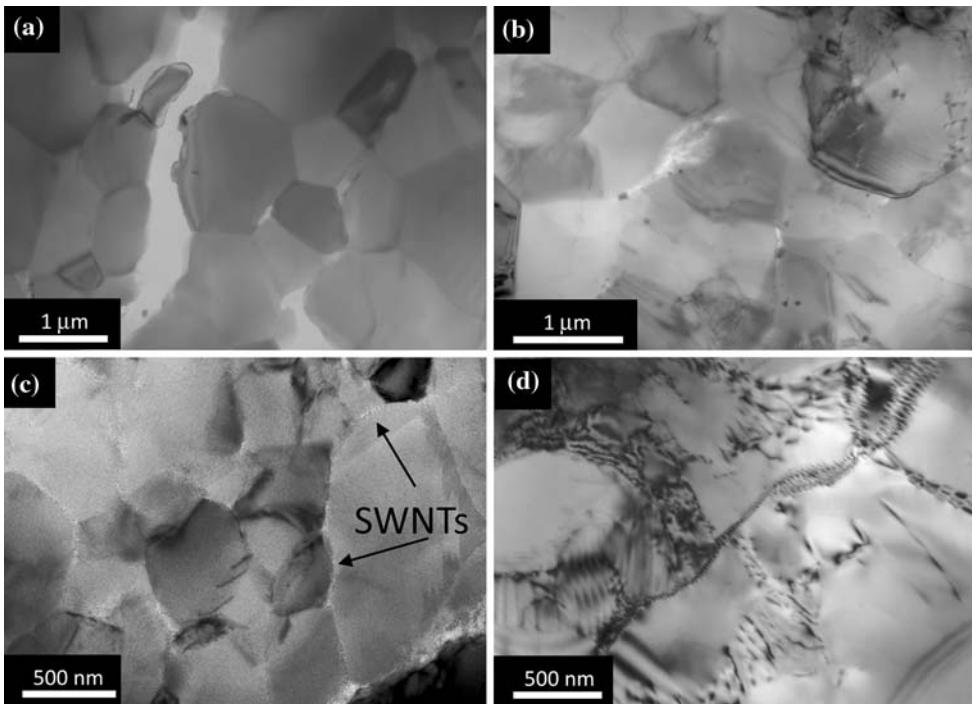

Fig. 5 Bright Field TEM picture of **a** Al_2O_3/SWNTs before deformation. **b** Al_2O_3/SWNTs after deformation. **c** Al_2O_3/TSWNTs before deformation. **d** Al_2O_3/TSWNTs after deformation

$$\dot{\varepsilon} = \rho b V \tag{10}$$

With the substitution of Eqs. 8 and 9 into Eq. 10, next equation is obtained,

$$\dot{\varepsilon} = K\Phi\sigma^3 \frac{D_{\text{eff}}}{kT} \tag{11}$$

where K is a material constant.

In our materials, a stress exponent close to 3 has been measured. Therefore, the Eq. 11 allows us to explain the mechanical behaviour of our composites. Figure 6 is a plot of steady-state strain rate versus stress normalised by surface fraction of Al_2O_3 grains surface without contact with SWNTs Φ. Good fit can be observed between experimental data and the model developed. Notice that a stress exponent lower than 3 has been measured due to some grain boundary sliding. Recently a new model developed by our group [35], has put forward a theoretical approach to grain boundary sliding in ceramics systems, without the presence of dislocation activity during deformation, as it is observed in most polycrystalline ceramics as YTZP [36], MgO [37] and β-SiAlON [38]. Arising from this model a stress exponent of 2 is explained for grain boundary sliding during deformation. The grain boundary sliding mechanism can be explained as the consequence of the peculiar compromise between grain dynamics and mass transport among grains when the material is mechanically stressed. In the Al_2O_3/SWNTs and Al_2O_3/TSWNTs composites, SWNTs inhibit

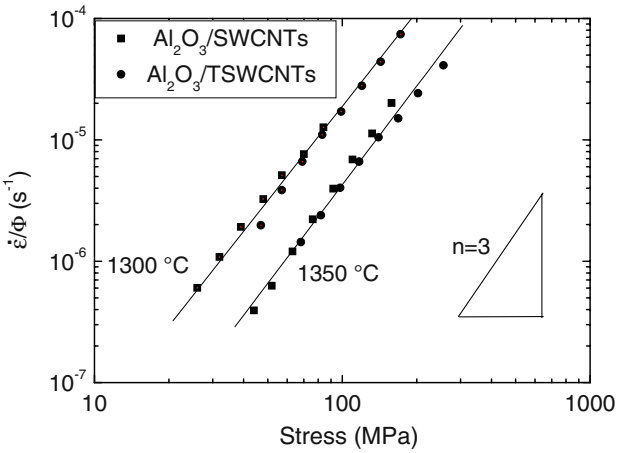

Fig. 6 Theoretical analysis of high-temperature creep data of Al_2O_3/SWCNTs and Al_2O_3/TSWCNTs composites

diffusion partially along grain boundaries and blocked grain boundary sliding, subsequently a harder mechanism as recovery creep take place. Nevertheless, marginal grains may slide resulting in a stress exponent lower than 3.

Conclusions

Ceramic/SWCNTs composites properties are related with the unique grain boundary structure. A geometrical model

of SWNT distribution along grain boundaries has been developed to study the relationship between the different quantitative SWCNTs distribution magnitudes measured in a previous study [28]. The model gives a good accuracy of the ratio of SWCNTs in contact with alumina grains. Therefore, this model can be of great help for ongoing works to correlate physical properties with SWCNTs ceramic matrix composites microstructure.

Acknowledgements The authors acknowledge the financial support awarded by the Spanish "Ministerio de Ciencia e Innovación" through the Grant MAT2006-10249-C02-02 and MAT2009-14351-C02-01. E. Zapata-Solvas would like to acknowledge the financial support awarded by the "Fundación Ramón Areces" during his postdoctoral stay at Imperial College London. Special acknowledgement must be extended to Prof. N. P. Padture, Dr. R. Poyato, Prof. V. Radmilovic and Dr. Z. Lee for fruitful discussion.

References

1. Iijima S (1991) Nature 354:56
2. Treacy MMJ, Ebbesen TW, Gibson JM (1996) Nature 381:678
3. Odom TW, Huang JL, Kim P, Lieber CM (1998) Nature 391:62
4. Ebbesen TW, Lezec HJ, Hiura H, Bennett JW, Ghaem HF, Thio T (1996) Nature 382:54
5. Kataura H, Kumazawa Y, Maniwa Y, Umezu I, Suzuki S, Ohtsuka Y, Achiba Y (1999) Synth Met 103:2555
6. Wang XT, Padture NP, Tanaka H (2004) Nature Mater 3:539
7. Zapata-Solvas E, Poyato R, Gómez-García D, Domínguez-Rodríguez A, Radmilovic V, Padture NP (2008) Appl Phys Lett 92:111912
8. Zhan GD, Kuntz JD, Garay JE, Mukherjee AK (2003) Appl Phys Lett 83:1228
9. Tatami J, Katashima T, Komeya K, Meguro T, Wakihara T (2005) J Am Ceram Soc 88:2889
10. Zhan GD, Kuntz JD, Wang H, Wang CM, Mukherjee AK (2004) Philos Mag Lett 84:419
11. Zhan GD, Kuntz JD, Mukherjee AK, Zhu P, Koumoto K (2006) Scripta Mater 54:77
12. Iijima S, Brabec C, Maiti A, Bernholc Z (1996) J Phys Chem 104:2089
13. Calvert P (1999) Nature 399:210
14. Yu MF, Files BS, Arepalli S, Ruoff RS (2000) Phys Rev Lett 84:5552
15. Baughman RH, Zakhidov AA, deHeer WA (2002) Science 297:787
16. Chiang YM, Birnie D, Kingery WD (1997) Physical ceramics: principles for ceramic science and engineering. Wiley, New York
17. Salvetat JP, Briggs GAD, Bonard JM, Bacsa RR, Kulik AJ, Stockli T, Burnham NA, Forro L (1999) Phys Rev Lett 82:944
18. Kis A, Csanyi G, Salvetat JP, Lee TN, Couteau E, Kulik AJ, Benoit W, Brugger J, Forro L (2004) Nature Mat 3:153
19. Poyato R, Vasiliev AL, Padture NP, Tanaka H, Nishimura T (2006) Nanotechnology 17:1770
20. Sun J, Gao L, Li W (2002) Chem Mater 14:5169
21. Balazsi C, Konya Z, Weber F, Biro LP, Arato P (2003) Mater Sci Eng C 23:1133
22. Balazsi C, Sedlackova K, Czigany Z (2008) Compos Sci Technol 68:1596
23. Konya Z, Vesselenyi I, Niesz K, Kukovecz A, Demortier A, Fonseca A, Delhalle J, Mekhalif Z, Nagy JB, Koos AA, Osvath Z, Kocsonya A, Biro LP, Kiricsi I (2002) Chem Phys Lett 360:429
24. An LN, Xu WX, Rajagopalan S, Wang C, Wang H, Fan Y, Zhang LG, Jiang DP, Kapat J, Chow L, Guo BH, Liang J, Vaidyanathan R (2004) Adv Mater 16:2036
25. Vasiliev AL, Poyato R, Padture NP (2007) Scripta Mater 56:461
26. Koszor O, Tapaszto, Marko M, Balazsi C (2008) Appl Phys Lett 93:201910
27. Zhan GD, Kuntz JD, Wan J, Mukherjee AK (2003) Nature Mater 2:38
28. Zapata-Solvas E, Gómez-García D, Poyato R, Lee Z, Castillo-Rodríguez M, Domínguez-Rodríguez A, Radmilovic V, Padture NP (2009) J Am Ceram Soc (accepted)
29. Xue LA, Chen IW (1990) J Am Ceram Soc 73:3518
30. Zapata-Solvas E (2008) PhD Thesis, University of Seville, Department of Condensed Matter Physics
31. Poirier JP (1985) Creep of crystals. Cambridge University Press, Cambridge
32. Friedel J (1964) Dislocations. Pergamon Press, Oxford
33. Pletka BJ, Heuer AH, Mitchell TE (1977) Acta Metall 25:25
34. Bretheau T, Castaing J, Rabier J, Veyssiere P (1979) Adv Phys 28:835
35. Gómez-García D, Zapata-Solvas E, Domínguez-Rodríguez A, Kubin L (2009) Phys Rev B 80:214107
36. Zapata-Solvas E, Gomez-Garcia D, Garcia-Ganan C, Dominguez-Rodriguez A (2007) J Eur Ceram Soc 27:3325
37. Dominguez-Rodriguez A, Gomez-Garcia D, Zapata-Solvas E, Shen JZ, Chaim R (2007) Scripta Mater 56:89
38. Chihara K, Hiratsuka D, Shinoda Y, Akatsu T, Wakai F, Tatami J, Komeya K (2008) Mater Sci Eng B 148:203